Sensitivity of urban heat islands to various methodological schemes

Gemechu Fanta Garuma *[1]

[1] *Entoto Observatory and Research Center (EORC), Atmospheric and Climate (AtClim) Sciences Unit, Department of Space and Planetary Sciences at the Space Science and Geospatial Institute (SSGI), Addis Ababa, Ethiopia.*

Abstract

Existing research has employed various methods to quantify urban heat island (UHI) effects, but the ideal method for individual cities remains unclear. This study investigated how different methods influence UHI understanding in Addis Ababa, a tropical city facing UHI challenges. Three methods were compared: dynamic urbanization, natural and built-up fractions, and urban center vs. surrounding rural areas. Satellite data and spatial analyses revealed maximum daytime UHIs of 4°C and 3.1°C in summer and autumn, respectively. Examining the mean temperature differences between urban and rural areas across methods yielded diverse results. This suggests that while the 'dynamic urbanization' method is statistically favorable in this specific case, averaging results from multiple methods produced a more robust and generalizable approach to understanding UHIs in different urban contexts. Ultimately, this study highlights the importance of context-specific method selection for accurately understanding the complex interplay between urban and rural environments.

keywords: urban heat islands; methods; urban climate; dynamic urbanization; land cover; natural and urban fractions

1 Introduction

World urban population is estimated to rise from the current 55% to 68% by 2050, out of which the nearly 90% increase will come from Asia and Africa (UN (2022)). This urbanization requires careful planning to accommodate people and to adapt to the consequences of urban climate under a changing environment. The urban environments are found to be warmer than rural areas (Oke (1982); Ferguson and Woodbury (2007); Oleson et al. (2011); Clinton and Gong (2013); Garuma et al. (2018); Kim and Brown (2021)) known as the urban heat island effect. Complemented with global warming, it puts the urban water and energy under a high constraint (McCarthy et al. (2010)). That is the combined overheating from the urban heat islands and global warming induced heat waves have adverse effects on human health and the urban biosphere.

The urban heat island (UHI) impacts more than just temperature. It alters precipitation patterns (Dixon and Mote (2003); Li et al. (2020)), fuels flash floods through intense thunderstorms (Qiu (2012); Ntelekos et al. (2007)), and even affects regional plant growth (Shochat

*Corresponding author: Gemechu Fanta Garuma, Research Scientist and Assistant Professor, email: gemechuf@essti.gov.et & gemechufanta@gmail.com

et al. (2006)). To mitigate these effects, understanding UHI and its sensitivity to different measurement methods is crucial. While urban layout and materials significantly influence UHI intensity (Liu et al. (2021); Steeneveld et al. (2011); Liao et al. (2021); Liu et al. (2020b); Yin et al. (2018); Touchaei and Wang (2015); Stone Jr and Rodgers (2001); Santos et al. (2021))n, no prior studies have compared various UHI calculation methods for sensitivity analysis. Existing research on UHI often compares urban and rural weather data (Wang et al. (1990); Roth (2012); Oke (2010); Garuma (2022)). This can be done in three ways: comparing urban centers to surrounding rural areas (Fig. S1), analyzing natural vs. built-up areas within the same grid (Fig. S2), or tracking UHI changes over time (Fig. S3).

This first method compares urban and rural grids directly (Fig. S1 (a)) (e.g., Garuma et al. (2018); Myrup (1969)). It chooses nearby grids to isolate the impact of the city from broader climate changes. Mean temperatures are then compared between the central urban grid and surrounding rural grids in different directions (Fig. S1 (b)). This is often applied in specific rectangular or circular areas within the city and surrounding countryside.

The second method compares urban and rural fractions within a single grid (Fig. S2). Often used in weather models (e.g., Li and Bou-Zeid (2014); Kusaka et al. (2012); Oleson et al. (2008)), it involves two simulations: one with an "urban canopy model" (Fig. S2 (b)) and another without (Fig. S2 (a)). Alternatively, real-world data such as earth observation information or ground measurements can be filtered based on urban and rural fractions (e.g., buildings vs. vegetation)(e.g., Tran et al. (2006); Singh et al. (2022); Zhou et al. (2010)). This requires land cover data and statistical techniques to identify urban and rural grids.

The third method, less common but crucial, tracks UHI changes over time (e.g., Ogashawara and Bastos (2012); Dutta et al. (2021); Liu et al. (2019)). It incorporates urban development into climate models, simulating how weather changes with city growth. This helps understand current UHI impacts and predict future effects, especially for land-use transitions (rural to urban or vice versa). While requiring detailed data on building properties and land-use changes, this method offers valuable insights for urban planning and adaptation, remembering to account for separate effects of global warming.

Another rare approach compares pre-existing and post-construction climates (e.g., Beijing's Olympic expansion (Sun and Chen (2017); Liu et al. (2020a); Meng et al. (2018)). This leverages new city development, hypothetical pre-city scenarios, or disaster reconstruction (Renard et al. (2019)). It's also useful for studying urban redevelopment impacts or even individual building projects, revealing localized weather and climate changes.

Another approach uses scenarios to predict future UHI impacts based on changes in urban fractions like building coverage, roads, vegetation, and even solar panels. This helps compare past, present, and future trends or model different development scenarios (low, medium, high) or specific urban climate zones (Stewart and Oke (2012)). Analyzing these fractional changes reveals how different land use changes interact with local weather and climate.

Human activities also influence UHI, and anthropogenic heat and moisture emissions are also used to understand the impacts of human settlements (Shahmohamadi et al. (2011); Kato and Yamaguchi (2005); Ichinose et al. (1999)). Methods like comparing weekdays and weekends separate human-caused heat from solar effects (Kim and Baik (2005); Earl et al. (2016); Wang et al. (2022); Ngarambe et al. (2021); Nwaerema and Jiya (2021)). Similarly, comparing early mornings with later daytime conditions isolates the built environment's impact (Giannaros et al. (2013); Lehoczky et al. (2017)). These methods require detailed data on energy use, population, and other urban heat sources, but offer valuable insights into the combined effects of urban infrastructure and human activity on local weather and climate.

Despite a plethora of studies applying various methods to calculate urban climate, a crucial piece is missing: a comparative analysis of their outputs. This research fills this void by evaluating three prevalent methods used by urban climate researchers. These are: (1) comparing the urban center to surrounding rural areas (Fig. S1 (b)), 2) analyzing the fractions of natural and built-up land cover (Fig. S2 (b)), and 3) exploring the temporal dynamics of urban land cover changes (Fig. S3 (a) and (b)). Accordingly, this paper examines the spatio-temporal characteristics of Tropical Surface Urban Heat Islands (TSUHIs) (Garuma (2023)) in a specific East African city. It employs three widely used methodologies, aiming to: (1) analyze and characterize the city's TSUHIs through diverse methodological approaches; (2) evaluate the performance and accuracy of each method against observational data; and (3) identify the optimal method for effectively determining the spatio-temporal patterns of TSUHIs in this specific tropical city. The paper is organized as follows: it commences with materials and data analysis methods (Section 2), delves into detailed results and discussion (Section 3), and culminates with the study's overarching conclusions (Section 4).

2 Materials and methods

2.1 Study area

This study evaluates three UHI calculation methods in Addis Ababa, Ethiopia (35.5^oE - 39^oE, 8.7^oN - 9.2^oN). The rapidly growing city (urban cover 0% to 95%) (Fig. 1) experienced real estate booms expanding westward and eastward (2005-2015) (Mohamed and Worku (2019)). This rapid change prompted the study to compare methods for effective urban climate analysis in such scenarios. Addis Ababa, the most populous Ethiopian city, houses the African Union and other organizations. Its complex topography ranges from 2,300m to 3,200m above sea level. It has moderate temperatures (10^oC to 30^oC) with a wet summer and dry winter. Spring brings the rainy season, while summer is the wettest for the highlands, followed by drier autumn and winter (Diro et al. (2011)).

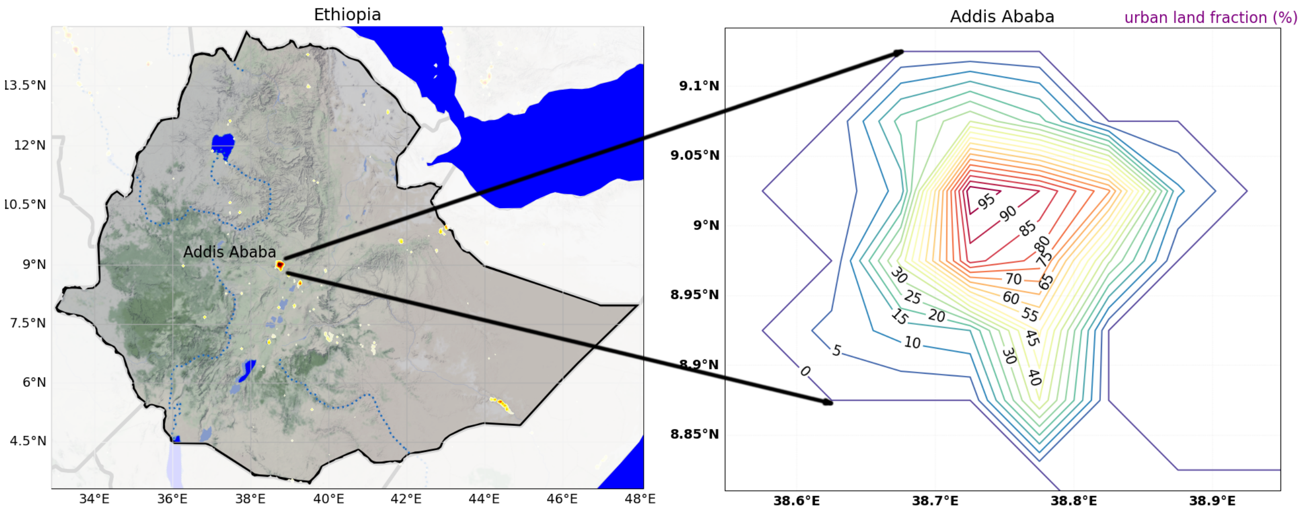

Figure 1: This map reveals the varying levels of urban development around and within Addis Ababa. Contour lines with increasing color intensity depict a gradient in urban density, with blue representing 0% at the city's periphery and deep red signifying 95% in the central areas.

2.2 Data sources

This study utilized daily and monthly land surface temperature and land cover data from the MODIS sensor (0.05^o resolution) for the period 2000-2020 (Wan et al. (2015)). MODIS land cover data helped identify urban and rural fractions within each grid cell (Fiedl and Sulla-Menashe (2015)). To ensure accuracy, MODIS land surface temperature data was bias-corrected and validated against measurements from meteorological stations in Addis Ababa, including Bole International Airport and the Ethiopian Meteorological Institute's main office. The temperature data from the meteorological stations was obtained from the National Meteorological Agency (`http://www.ethiomet.gov.et/data_access/information`) and the Berkley Earth Database (`https://data.berkeleyearth.org/locations/8.84N-38.11E`).

2.3 Bias correction

MODIS land surface temperature data contained a bias compared to ground stations. To address this, the satellite data was bias-corrected using station observations from the nearest grid point. Station data was first filtered for outliers using the median filter outliers method (Lim (1990)) and then used to calculate a correction factor based on the average temperature difference between MODIS and station data. That is,

$$T_{BC}(t) = T_M(t) + (\overline{T_O} - \overline{T_M}) \tag{1}$$

where the T_{BC}, T_M and T_O are the bias corrected (BC) land surface temperature (LST), the MODIS LST and station observation temperatures respectively.
This correction was applied to the MODIS data, resulting in a bias-corrected version (T_{BC}). The effectiveness of the correction was assessed by comparing the spatial pattern of the bias-corrected MODIS data with the station observations. Pattern similarity correlation between the observation LST (T_O) and the bias-corrected MODIS LST (T_M) is

$$R = \frac{\frac{1}{N}\sum_{n=1}^{N}(T_M - \overline{T_M})(T_O - \overline{T_O})}{\sigma_{T_M}\sigma_{T_O}}, \tag{2}$$

where $\overline{T_M}$ and $\overline{T_O}$ are the mean values and σ_{T_M} and σ_{T_O} are their respective standard deviations. The correlation coefficient reaches a maximum value of 1 when the two data sets have the same centered pattern, otherwise the R values are less than 1. A high correlation coefficient indicated successful correction.

2.4 Tropical surface urban heat islands

This study compares three established methods for examining urban climate: 1) natural vs. built-up fractions, 2) urban centers vs. surrounding rural areas, and 3) dynamic changes over time.

Method 1: Natural vs. built-up fractions

This method uses land cover fractions (vegetation vs. urban) to identify urban and rural areas (Fig. S4). Urban fractions are higher in the city center, while vegetation dominates the outskirts. TSUHI is calculated as the difference in land surface temperature (LST) between grids with high urban and high vegetation fractions (LST urban - LST rural). Grids with ¿5% vegetation and ¡5% urban area are considered rural, while the opposite defines urban grids. The day/night TSUHI (TSUHI$_{d/n}$) is then determined by the LST difference between these categories, i.e.,

$$TSUHI_{(d/n)} = LST_{(d/n;u)} - LST_{(d/n;r)} \tag{3}$$

where LST$_{d/n,u}$ and LST$_{d/n,r}$ are the urban and rural LST respectively during the day and night (d/n). For the observation analysis the skin surface temperature from two meteorological observation sites at the airport and center of the city are used.

Method 2: Urban centers vs. surrounding rural areas

This method defines urban areas as a central region with high urban land cover (Fig. S4 (d)) surrounded by rural areas with more vegetation (Fig. S4 (e)). Figure S4 (f) shows the urban land cover (red shaded contours) overlayed within the urban domain and the surrounding rural fractions shown with more vegetation fractions (green contours). The surface urban heat island (SUHI) is calculated by comparing the average land surface temperature of the central urban area with the surrounding rural areas, similar to equation 3. This method uses a larger rural area than the previous method, leading to a higher average vegetation fraction (39% vs. 35%) (compare Figs. S4 (b) and (e)).

Method 3: Dynamic urbanization

This method tracks changes in urban land cover and vegetation over time to assess UHI impacts (Fig. S4 (c)). It compares the differences between early and later periods of rapid urbanization (2000-2010 vs. 2011-2020) using land cover (Fig. S4 (g)) and vegetation fractions (Fig. S4 (h)). As shown in Fig. S4 (i), the western and eastern city areas underwent significant expansion (red contours), highlighting the impact of recent development.
The surface urban heat island computed in this method is

$$TSUHI_{(d/n)} = LST_{(d/n;p2)} - LST_{(d/n;p1)} \tag{4}$$

where the (d/n) is the day or night values; $p1$ and $p2$ are the periods where there was low and high urban developments respectively. The period $p2$ is a later period than $p1$. For this study, p1 and p2 are the periods from 2000-2010 and 2011-2020 respectively.

2.5 Performance of the methods compared to the mean

The performance of each method in capturing UHI was assessed using standard deviation (SD), root mean square deviation (RMSD), and correlation coefficient (CC) compared to observations and a composite mean. Taylor diagrams (Taylor (2001)) and boxplots additionally evaluated the overall skill of each method. These metrics helped determine which method produced results closest to observations, indicating better performance for this specific city. This evaluation also helps understand how sensitive the methods are to UHI calculations. The priority lies in SD and RMSD, as high values indicate significant errors or outliers, even with a high CC.

3 Results and discussion

3.1 Bias correction and validation

Bias correction for MODIS data was performed using eqn. 1., leveraging observation data from the closest meteorological station. The correlation between the corrected MODIS and observation data was then calculated to evaluate the correction's impact on data suitability.
Bias correction significantly improved the agreement between MODIS data and station observations. Daytime and nighttime urban temperatures exhibited strong correlations, with R-squared values of 0.94 and 0.99, respectively (Figs. 2 (a) and (b)). Compared to nighttime data, daytime LST displayed a wider scatter around the mean and higher variability. Notably, the mean LST for both day and night achieved an R-squared value of 0.97 (Fig. 2 (c)). These findings demonstrate the high accuracy of the bias-corrected MODIS data for our research purposes. This implies that the data is well-suited to investigate the methodological sensitivities of urban heat island characteristics in this specific tropical city.

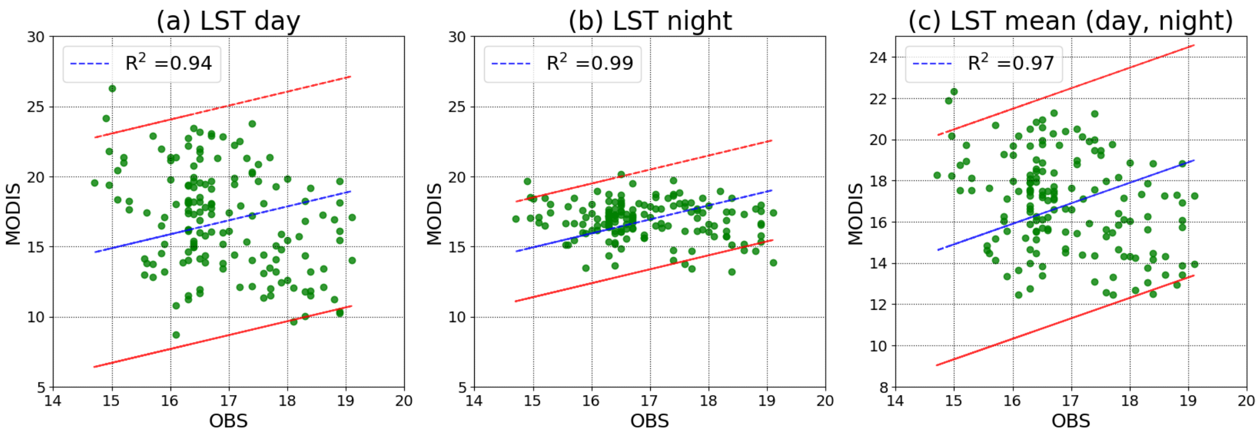

Figure 2: Validation of MODIS LST using stationary observation data for (a) day, (b) night and (c) mean of the day and night. The green dots are the actual data points calculated at 99.9% confidence interval under Ordinary Least Squares (OLS) assumptions. The blue line in the middle is the linear least squares fit with an indicated R-squared values. The upper and lower red lines are for the upper an lower bounds respectively at 99.9% confidence level.

3.2 Representing tropical surface urban heat islands

This study aims to challenge the misconception that tropical cities in developing countries lack urban heat islands (UHIs). This belief stems from the inhomogeneous distribution of buildings and roads in sub-Saharan African cities, where skyscrapers often stand alongside informal settlements. However, the rapid urbanization in these regions, driven by the desire for better education, healthcare, and employment, leads to increased water and energy consumption, releasing anthropogenic heat and moisture into the environment. Despite the spatial heterogeneity, roads, sidewalks, and other impervious surfaces contribute significantly to altering the energy and moisture balance compared to rural areas. These changes, coupled with dense populations and consequent human activities, create distinct weather and climatic conditions, potentially leading to UHIs even in seemingly inhomogeneous landscapes.

Our analysis confirms the presence of Tropical Surface Urban Heat Islands (TSUHIs) in this sub-Saharan African city during summer and autumn seasons (Fig. 3). In these seasons, the central city exhibits significantly higher daytime Land Surface Temperatures (LSTs) compared to its outskirts. As shown in Figs. 3 (c) and (d)), the summer LST reaches 27.5°C at the center, while the edges experience cooler temperatures around 23.5°C. Similarly, autumn daytime LSTs peak at 30.6°C in the center, contrasting with 27.5°C at the city's periphery.

These temperature differences are visualized by the closed contour lines in Fig.3 radiating outwards from the warmer center. We estimated the TSUHI intensity by subtracting the LST at the city edges from the central values. This reveals a summer TSUHI of 4°C and an autumn TSUHI of 3.1°C, signifying that the city center is warmer than surrounding rural areas during these seasons.

However, the analysis for winter and spring seasons (not shown) doesn't show similar patterns. Instead, temperature variations follow a latitudinal trend, where temperatures are generally higher near the tropics and decrease at higher latitudes. Consequently, based on these spatial analyses, there are no night time surface temperature variations in all the seasons (Fig. S6) implying that there is no distinct tropical surface urban heat islands during the night in this city based on this spatial analysis.

The cool island in the north western part of the city is nearly adjacent to the city where there is a chain of mountains, as shown by the blue closed contour lines in Fig. 3. The city is surrounded

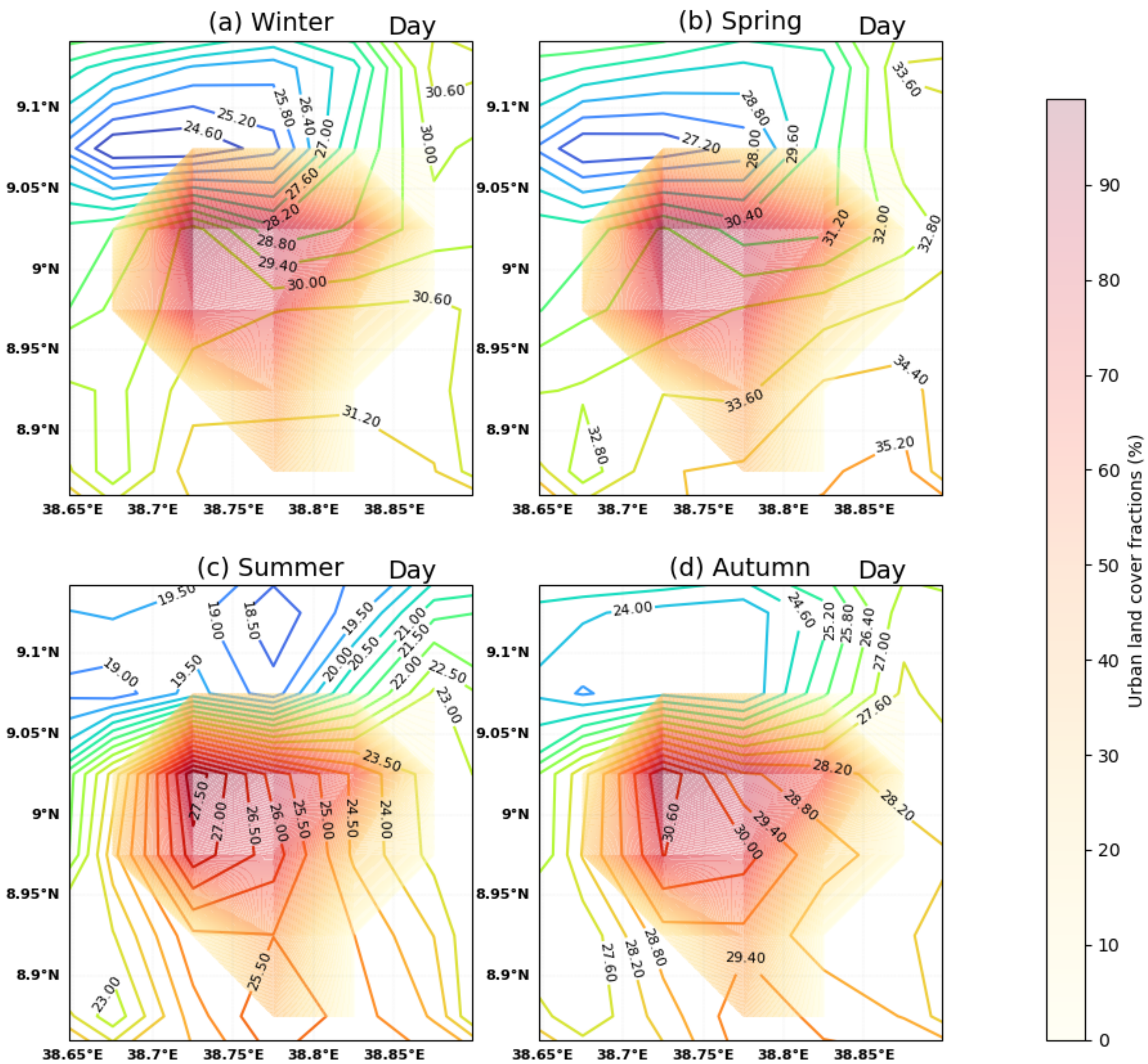

Figure 3: Seasonal mean (2000-2020) MODIS represented land surface temperature contour lines for (a) winter, (b) spring, (c) summer, and (d) autumn seasons during the day light time.

by a chain of Entoto mountains in the north where the peak of the mountain reaches 2300 m above sea level extending from the north east to the north west. Most of the terrain of this mountain is covered by eucalyptus trees. The closed blue contour lines in the northern part of the city show cooler islands as a result of the higher topography. In winter, the mountains are colder by at least 3^{o}C, that is from 27.6^{o}C at the edge of the cold center to 24.6^{o}C at the center. In autumn, it is 3.2^{o}C, that is taking the difference from the edge to the center, 30.4^{o}C-27.2^{o}C. The cold center in summer and autumn are around 0.5^{o}C in the Northern part of the city. The center of the city didn't show closed isothermal lines during these two seasons implying that there was no urban heat islands. Generally, the surface cool islands dominate in winter and spring in the northern part of the city pertaining to topographical variations. Furthermore, the tropical surface urban heat islands dominate in the center of the city during summer and autumn seasons.

While spatial analysis offers insights into temperature gradients (Fig. 3), it isn't enough to fully understand the overall impact of urban heat islands (UHIs). Analyzing the mean temperature difference between urban and rural areas provides a more comprehensive picture. Therefore, the area-averaged seasonal temperature differences were calculated between urban and rural areas using three methods: urban and rural fractions within each grid cell (Fig. S5 (a)), urban center vs. surrounding rural areas (Fig. S5 (b)), and urban dynamics (Fig. S5 (c)). After identifying urban and rural Land Surface Temperatures (LSTs), their difference provides the Tropical Surface Urban Heat Islands (TSUHIs). Interestingly, results reveal both heat and cool islands depending on the season (Fig. S5 (d)): TSUHIs are observed in summer and autumn (JJA-SON) seasons with the city experiencing heat islands up to 1.7^{o}C warmer than surrounding areas (Fig. S5 (d)). The city transitions to a cool island from winter to spring (DJF-MAM), with temperatures as much as 1.8°C cooler than rural areas.

While methods 1 (red line) and 2 (blue lines) in Fig. S5 (d) show similar patterns, method 3 (orange line) deviates significantly during winter. This suggests that methods 1 and 2 are more consistent in capturing the overall TSUHI pattern, except during winter. However, relying solely on temporal observations makes it challenging to definitively identify the best performing method. Therefore, the next section will employ a different approach for a more comprehensive evaluation.

3.3 Sensitivity of the methods to represent TSUHIs

This study delves into whether the representation of urban heat islands (UHIs) hinges on the specific method employed, or if all methods yield identical results. Understanding this methodological sensitivity is crucial for the urban climate research community. This analysis reveals remarkable seasonal variations in the mean daytime TSUHIs calculated using three distinct methods (Table S1). For instance, summer TSUHIs range from 0.72^{o}C to 1.03^{o}C, while autumn values span from 0.30^{o}C to 1.29^{o}C. These significant discrepancies across methods highlight the critical dependence of UHI results on the chosen approach and the unique characteristics of the studied urban area. In light of these diverse outcomes, a meticulous evaluation of each method becomes essential to determine its suitability and limitations for representing UHIs in different contexts.

To assess the sensitivity of each method in capturing Tropical Surface Urban Heat Islands (TSUHIs), we employed two key tools: taylor diagram (Taylor (2001)) (Fig. 4 (a)) and box plots (Fig. 4 (b)). By combining these tools, we gain a comprehensive understanding of how each method responds to the complexities of TSUHI representation, ultimately guiding the selection of the most suitable approach for specific research contexts.

Analyzing the Taylor diagram (Fig. 4 (a)), Method 3 stands out in capturing TSUHI amplitude variations due to its comparable standard deviation with observation data. Despite a high

offset (RMSD), its strong correlation (≅ 0.35) suggests a consistent overestimation. Method 2 performs moderately with an intermediate correlation, while Method 1 shows the weakest relationship with observed values, indicating its relative inferiority.
While Method 3 captures TSUHI variations well (Fig. 4 (a)), its overestimation is evident. Both Methods 1 and 2 underestimate TSUHIs (Fig. 4 (b)). Interestingly, the average of all methods (Mean(M1, M2, M3)) shows the best performance due to its minimal spread and symmetrical distribution. This suggests its suitability for representing TSUHIs in similar rapidly urbanizing cities, like Addis Ababa (Fig. 4). This aligns with findings from other studies highlighting the city's rapid expansion in recent years (Mohamed and Worku (2019),Debelo and Soboka (2022)), making this method a potential choice for analyzing TSUHIs in similar contexts.

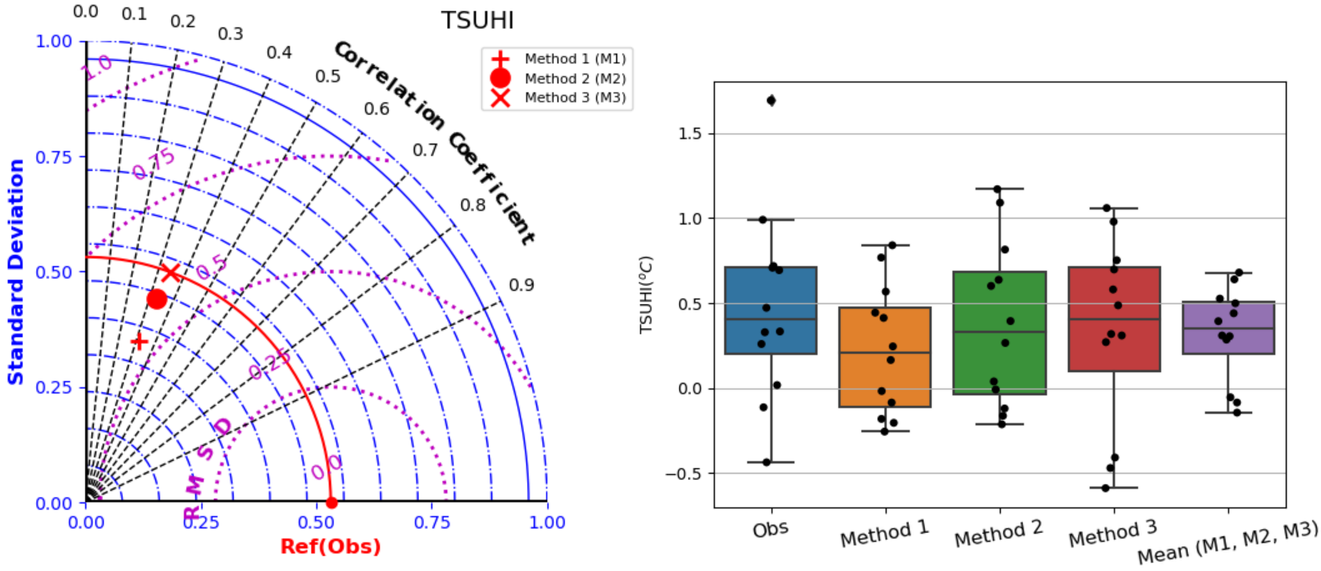

Figure 4: The performance evaluation of the computation methods M1, M2, and M3 relative to the observation in representing the tropical surface urban heat islands using (a) Taylor diagram and (b) box plots.

In conclusion, while averaging diverse methods offers robust urban heat island (TSUHI) information, specific historical contexts can guide method selection. In rapidly expanding cities, the "current vs. past urban morphology" approach excels. Stable, low-growth environments benefit from methods comparing vegetation to impervious surfaces or urban cores to rural areas. Conversely, areas implementing mitigation like vegetation or albedo changes thrive with the "fractional changes in imperviousness, vegetation, and albedo" method for accurate weather and climate estimation.

4 Conclusion

This study investigated the nature of tropical surface urban heat islands (TSUHIs) using qualitative spatial analysis and quantitative temporal analysis. The spatial analysis employed shaded or unshaded contour lines to map temperature gradients from the city center to its outer edges. This visualization revealed how different parts of the city heated up compared to surrounding rural areas. However, this method wasn't sufficient to capture the combined impacts of urban surfaces on weather and climate over time. To address this limitation, the study incorporated area-averaged temporal analysis. This technique computed the average temperature within the entire urban area over a specific period. This produced a cumulative view of how the entire

city, as a whole, affects surrounding weather and climate patterns compared to rural areas. By combining these distinct analyses, the study paints a more comprehensive picture of TSUHIs in tropical cities.
To comprehensively understand the cumulative effects of tropical surface urban heat islands (TSUHIs) in Addis Ababa, the study employed three established urban climate estimation methods:

- M1: Natural and built-up fractions: This method differentiates urban and rural areas based on land cover and vegetation fractions. Urban areas typically have less vegetation and more impervious surfaces, which is expected to result in higher heat retention and warmer temperatures.
- M2: Urban center vs. surrounding rural areas: This method focuses on the temperature contrast between the urban center, considered the hottest zone, and the surrounding rural areas. This approach highlights the localized heat island effect within the city.
- M3: Urban dynamics: This method analyzes land cover transitions from rural to urban over time and space. By tracking these changes, it is possible to understand how urban expansion and development contribute to rising temperatures and altered climate patterns.

A qualitative spatial analysis of this tropical city revealed the presence of surface urban heat islands in summer and early autumn, peaking at 4^{o}C and 3.1^{o}C respectively. This analysis compared the urban center's temperature grid to those at the city's edge, representing the maximum achievable heat island intensity. However, nighttime urban heat islands weren't detectable through this method alone. To gain a more comprehensive understanding, the study incorporated a composite mean value computation using three established methods, complementing the initial spatial analysis.
The mean TSUHI values vary depending on the method of computation under consideration. The two methods, M1 and M2 have almost similar patterns while method 3 is slightly different in capturing the seasonal variations of the TSUHIs. Nevertheless, all the methods show maximum heat islands in late summer and autumn (JJA-SON) seasons. As such, the surface urban heat islands in these seasons reach a maximum of 1.7^{o}C. The cool island reaches a minimum of -1.8^{o}C during the spring (MAM) season. During the night time, the city exhibits surface urban heat islands all the time except during the August month. The night time surface urban heat islands during the early autumn and early winter seasons reach a maximum of 1.2^oC. The cool island in August reaches a minimum of -0.4^{o}C. Nevertheless, the surface urban heat islands dominate the cool islands during the day and night times. The mean TSUHIs obtained using the three methods are 0.72^{o}C, 1.03^{o}C, and 0.74^{o}C in the summer, and 0.92^{o}C, 1.29^{o}C and 0.30^{o}C in the autumn seasons, implying that the results are sensitive to the methods used and are dependent on the characteristics of the specific urban area.
The study went beyond simply identifying the presence of urban heat islands. It also aimed to determine which method among the three employed was most effective in representing the city's unique urban climate. To achieve this, this study utilized Taylor diagrams and box plots. As such, the analysis revealed that the mean composite of all the three methods collectively offered the best representation of the citi's urban climate. This suggests that combining diverse approaches can yield more accurate results compared to relying on a single method. However, among the individual methods, method 3, which considered dynamic urbanization (land cover transitions from rural to urban), consistently outperformed the others. This indicates that for rapidly growing cities like the one studied, methods that account for the evolving urban landscape are particularly valuable.

The study emphasizes the benefits of using multiple methods to assess urban heat island characteristics. This allows for a more comprehensive understanding of the complex factors influencing urban climate. In cases where data limitations restrict the use of multiple methods, careful consideration of the city's development history is crucial for selecting the most suitable single method. This is specially advisable to urban climate studies in developing countries where the availability of data for the applicability of various methods is challenging. For cities experiencing rapid urban expansion, method 3, which leverages the dynamics of urbanization, is likely to provide the most accurate results. Similar performance can be expected in cities with comparable growth patterns. These findings highlight the importance of tailoring urban climate assessment methods to the specific characteristics of each city. As cities continue to grow and evolve, developing robust and adaptable methods for understanding and managing their unique climates will be essential.

Acknowledgments

The author thanks the Space Science and Geospatial Institute (SSGI) for funding this project under a project code ESSTI-SS-IP01-0120. Thanks to the Integrated Climate Data Center (ICDC), CEN, University of Hamburg for data support.

Data Availability

a. The MODIS land surface temperature and urban land fractions are obtained from the Integrated Climate Data Center (ICDC, icdc.cen.uni-hamburg.de) University of Hamburg, Hamburg, Germany. It is available freely for anyone from `https://www.cen.uni-hamburg.de/en/icdc.html`.

   - MODIS land surface temperature is available from `https://www.cen.uni-hamburg.de/en/icdc/data/land/modis-landsurfacetemperature.html`.
   - MODIS urban land surface fractions are extracted from `https://www.cen.uni-hamburg.de/en/icdc/data/land/modis-landsurfacetype.html`.

b. The temperature data from the meteorological stations was obtained from the National Meteorology Agency (`http://www.ethiomet.gov.et/data_access/information`) and the Berkley Earth Database (`https://data.berkeleyearth.org/locations/8.84N-38.11E`).

References

Clinton, N. and Gong, P. (2013). Modis detected surface urban heat islands and sinks: Global locations and controls. *Remote Sensing of Environment*, 134:294–304.

Debelo, A. R. and Soboka, T. E. (2022). Urban development and the making of frontiers in/from addis ababa/finfinne, ethiopia. *Journal of Asian and African Studies*, page 00219096211069647.

Diro, G. T., Toniazzo, T., and Shaffrey, L. (2011). Ethiopian rainfall in climate models. *African climate and climate change: physical, social and political perspectives*, pages 51–69.

Dixon, P. G. and Mote, T. L. (2003). Patterns and causes of atlanta's urban heat island–initiated precipitation. *Journal of Applied Meteorology*, 42(9):1273–1284.

Dutta, K., Basu, D., and Agrawal, S. (2021). Synergetic interaction between spatial land cover dynamics and expanding urban heat islands. *Environmental Monitoring and Assessment*, 193(4):1–22.

Earl, N., Simmonds, I., and Tapper, N. (2016). Weekly cycles in peak time temperatures and urban heat island intensity. *Environmental Research Letters*, 11(7):074003.

Ferguson, G. and Woodbury, A. D. (2007). Urban heat island in the subsurface. *Geophysical research letters*, 34(23).

Fiedl, M. and Sulla-Menashe, D. (2015). MOD11C1 MODIS/Terra Land Surface Temperature/Emissivity Monthly L3 Global 0.05Deg CMG V006. NASA EOSDIS Land Processes DAAC. `doi.org/10.5067/MODIS/MOD12C1.006`. [last accessed: November 30, 2020] - provided in netCDF file format by the Integrated Climate Data Center (ICDC, icdc.cen.uni-hamburg.de).

Garuma, G. F. (2022). How the interaction of heatwaves and urban heat islands amplify urban warming. *Advances in Environmental and Engineering Research*, 3(2):1–42.

Garuma, G. F. (2023). Tropical surface urban heat islands in east africa. *Scientific Reports*, 13(1):4509.

Garuma, G. F., Blanchet, J.-P., Girard, É., and Leduc, M. (2018). Urban surface effects on current and future climate. *Urban climate*, 24:121–138.

Giannaros, T. M., Melas, D., Daglis, I. A., Keramitsoglou, I., and Kourtidis, K. (2013). Numerical study of the urban heat island over athens (greece) with the wrf model. *Atmospheric Environment*, 73:103–111.

Ichinose, T., Shimodozono, K., and Hanaki, K. (1999). Impact of anthropogenic heat on urban climate in tokyo. *Atmospheric Environment*, 33(24-25):3897–3909.

Kato, S. and Yamaguchi, Y. (2005). Analysis of urban heat-island effect using aster and etm+ data: Separation of anthropogenic heat discharge and natural heat radiation from sensible heat flux. *Remote Sensing of Environment*, 99(1-2):44–54.

Kim, S. W. and Brown, R. D. (2021). Urban heat island (uhi) intensity and magnitude estimations: A systematic literature review. *Science of The Total Environment*, 779:146389.

Kim, Y.-H. and Baik, J.-J. (2005). Spatial and temporal structure of the urban heat island in seoul. *Journal of Applied Meteorology and Climatology*, 44(5):591–605.

Kusaka, H., Chen, F., Tewari, M., Dudhia, J., Gill, D. O., Duda, M. G., Wang, W., and Miya, Y. (2012). Numerical simulation of urban heat island effect by the wrf model with 4-km grid increment: An inter-comparison study between the urban canopy model and slab model. *Journal of the meteorological Society of Japan. Ser. II*, 90:33–45.

Lehoczky, A., Sobrino, J. A., Skoković, D., and Aguilar, E. (2017). The urban heat island effect in the city of valencia: a case study for hot summer days. *Urban Science*, 1(1):9.

Li, D. and Bou-Zeid, E. (2014). Quality and sensitivity of high-resolution numerical simulation of urban heat islands. *Environmental Research Letters*, 9(5):055001.

Li, L., Zha, Y., and Wang, R. (2020). Relationship of surface urban heat island with air temperature and precipitation in global large cities. *Ecological Indicators*, 117:106683.

Liao, W., Hong, T., and Heo, Y. (2021). The effect of spatial heterogeneity in urban morphology on surface urban heat islands. *Energy and Buildings*, 244:111027.

Lim, J. S. (1990). Two-dimensional signal and image processing. *Englewood Cliffs*.

Liu, H., Huang, B., Zhan, Q., Gao, S., Li, R., and Fan, Z. (2021). The influence of urban form on surface urban heat island and its planning implications: Evidence from 1288 urban clusters in china. *Sustainable Cities and Society*, 71:102987.

Liu, S., Zang, Z., Wang, W., and Wu, Y. (2019). Spatial-temporal evolution of urban heat island in xi'an from 2006 to 2016. *Physics and Chemistry of the Earth, Parts A/B/C*, 110:185–194.

Liu, X., Zhou, Y., Yue, W., Li, X., Liu, Y., and Lu, D. (2020a). Spatiotemporal patterns of summer urban heat island in beijing, china using an improved land surface temperature. *Journal of Cleaner Production*, 257:120529.

Liu, Y., Li, Q., Yang, L., Mu, K., Zhang, M., and Liu, J. (2020b). Urban heat island effects of various urban morphologies under regional climate conditions. *Science of the total environment*, 743:140589.

McCarthy, M. P., Best, M. J., and Betts, R. A. (2010). Climate change in cities due to global warming and urban effects. *Geophysical research letters*, 37(9).

Meng, Q., Zhang, L., Sun, Z., Meng, F., Wang, L., and Sun, Y. (2018). Characterizing spatial and temporal trends of surface urban heat island effect in an urban main built-up area: A 12-year case study in beijing, china. *Remote Sensing of Environment*, 204:826–837.

Mohamed, A. and Worku, H. (2019). Quantification of the land use/land cover dynamics and the degree of urban growth goodness for sustainable urban land use planning in addis ababa and the surrounding oromia special zone. *Journal of Urban Management*, 8(1):145–158.

Myrup, L. O. (1969). A numerical model of the urban heat island. *Journal of Applied Meteorology and Climatology*, 8(6):908–918.

Ngarambe, J., Joen, S. J., Han, C.-H., and Yun, G. Y. (2021). Exploring the relationship between particulate matter, co, so2, no2, o3 and urban heat island in seoul, korea. *Journal of Hazardous Materials*, 403:123615.

Ntelekos, A. A., Smith, J. A., and Krajewski, W. F. (2007). Climatological analyses of thunderstorms and flash floods in the baltimore metropolitan region. *Journal of Hydrometeorology*, 8(1):88–101.

Nwaerema, P. and Jiya, S. (2021). Evaluation of temperature and urban heat island variability in days of the week and weekends. *International Journal of Human Capital in Urban Management*, 6(1):45–56.

Ogashawara, I. and Bastos, V. d. S. B. (2012). A quantitative approach for analyzing the relationship between urban heat islands and land cover. *Remote Sensing*, 4(11):3596–3618.

Oke, T. R. (1982). The energetic basis of the urban heat island. *Quarterly Journal of the Royal Meteorological Society*, 108(455):1–24.

Oke, T. R. (2010). Urban heat islands. In *The Routledge handbook of urban ecology*, pages 144–155. Routledge.

Oleson, K. W., Bonan, G. B., Feddema, J., and Jackson, T. (2011). An examination of urban heat island characteristics in a global climate model. *International Journal of Climatology*, 31(12):1848–1865.

Oleson, K. W., Bonan, G. B., Feddema, J., and Vertenstein, M. (2008). An urban parameterization for a global climate model. part ii: Sensitivity to input parameters and the simulated urban heat island in offline simulations. *Journal of Applied Meteorology and Climatology*, 47(4):1061–1076.

Qiu, J. (2012). Urbanization contributed to beijing storms. *Nature*, 10.

Renard, F., Alonso, L., Fitts, Y., Hadjiosif, A., and Comby, J. (2019). Evaluation of the effect of urban redevelopment on surface urban heat islands. *Remote Sensing*, 11(3):299.

Roth, M. (2012). -urban heat islands. In *Handbook of Environmental Fluid Dynamics, Volume Two*, pages 162–181. CRC Press.

Santos, L. G., Nevat, I., Pignatta, G., and Norford, L. K. (2021). Climate-informed decision-making for urban design: Assessing the impact of urban morphology on urban heat island. *Urban Climate*, 36:100776.

Shahmohamadi, P., Che-Ani, A., Maulud, K., Tawil, N., and Abdullah, N. (2011). The impact of anthropogenic heat on formation of urban heat island and energy consumption balance. *Urban Studies Research*, 2011.

Shochat, E., Warren, P. S., Faeth, S. H., McIntyre, N. E., and Hope, D. (2006). From patterns to emerging processes in mechanistic urban ecology. *Trends in ecology & evolution*, 21(4):186–191.

Singh, P., Sarkar Chaudhuri, A., Verma, P., Singh, V. K., and Meena, S. R. (2022). Earth observation data sets in monitoring of urbanization and urban heat island of delhi, india. *Geomatics, Natural Hazards and Risk*, 13(1):1762–1779.

Steeneveld, G.-J., Koopmans, S., Heusinkveld, B., Van Hove, L., and Holtslag, A. (2011). Quantifying urban heat island effects and human comfort for cities of variable size and urban morphology in the netherlands. *Journal of Geophysical Research: Atmospheres*, 116(D20).

Stewart, I. D. and Oke, T. R. (2012). Local climate zones for urban temperature studies. *Bulletin of the American Meteorological Society*, 93(12):1879–1900.

Stone Jr, B. and Rodgers, M. O. (2001). Urban form and thermal efficiency: how the design of cities influences the urban heat island effect. *American Planning Association. Journal of the American Planning Association*, 67(2):186.

Sun, R. and Chen, L. (2017). Effects of green space dynamics on urban heat islands: Mitigation and diversification. *Ecosystem Services*, 23:38–46.

Taylor, K. E. (2001). Summarizing multiple aspects of model performance in a single diagram. *Journal of Geophysical Research: Atmospheres*, 106(D7):7183–7192.

Touchaei, A. and Wang, Y. (2015). Characterizing urban heat island in montreal (canada)—effect of urban morphology. *Sustainable Cities and Society*, 19:395–402.

Tran, H., Uchihama, D., Ochi, S., and Yasuoka, Y. (2006). Assessment with satellite data of the urban heat island effects in asian mega cities. *International journal of applied Earth observation and Geoinformation*, 8(1):34–48.

UN (2022). 68% of the world population projected to live in urban areas by 2050, says U. `https://www.un.org/development/desa/en/news/population/2018-revision-of-world-urbanization-prospects.html`. [Online; accessed 07-Feb-2022].

Wan, Z., H., S., and Hulley, G. (2015). MOD11C1 MODIS/Terra Land Surface Temperature/Emissivity Monthly L3 Global 0.05Deg CMG V006. NASA EOSDIS Land Processes DAAC. `doi.org/10.5067/MODIS/MOD11C3.006`. [last access date: May 26 2020], distributed in netCDF format by the Integrated Climate Data Center (ICDC, icdc.cen.uni-hamburg.de) University of Hamburg, Hamburg, Germany.

Wang, C., Zhan, W., Liu, X., Liu, Z., Miao, S., Du, H., Li, J., Wang, C., Li, L., and Yue, W. (2022). Strong modulation of human-activity-induced weekend effect in urban heat island by surface morphology and weather conditions. *Journal of Geophysical Research: Atmospheres*, 127(17):e2022JD036905.

Wang, W.-C., Zeng, Z., and Karl, T. R. (1990). Urban heat islands in china. *Geophysical Research Letters*, 17(13):2377–2380.

Yin, C., Yuan, M., Lu, Y., Huang, Y., and Liu, Y. (2018). Effects of urban form on the urban heat island effect based on spatial regression model. *Science of the Total Environment*, 634:696–704.

Zhou, J., Chen, Y., Wang, J., and Zhan, W. (2010). Maximum nighttime urban heat island (uhi) intensity simulation by integrating remotely sensed data and meteorological observations. *IEEE Journal of Selected Topics in Applied Earth Observations and Remote Sensing*, 4(1):138–146.

Seasons	Mean daytime TSUHI values			
	Method 1 (M1)	Method 2 (M2)	Method 3 (M3)	Mean(M1,M2,M3)
Summer	0.72^{o}C	1.03^{o}C	0.74^{o}C	0.83^{o}C
Autumn	0.92^{o}C	1.29^{o}C	0.30^{o}C	0.84^{o}C
Winter	-0.29^{o}C	-0.28^{o}C	0.89^{o}C	0.11^{o}C
Spring	-0.87^{o}C	-0.97^{o}C	-0.58^{o}C	-0.81^{o}C
Seasons	**Mean nighttime TSUHI values**			
	Method 1 (M1)	Method 2 (M2)	Method 3 (M3)	Mean(M1,M2,M3)
Summer	0.22^{o}C	0.33^{o}C	0.30^{o}C	0.28^{o}C
Autumn	0.53^{o}C	0.76^{o}C	0.30^{o}C	0.53^{o}C
Winter	0.81^{o}C	1.07^{o}C	0.89^{o}C	0.92^{o}C
Spring	0.56^{o}C	0.78^{o}C	-0.58^{o}C	0.25^{o}C

Table S1: This table shows the different mean TSUHI values for each of the methods, M1, M2, and M3. The observation TSUHI estimation and the mean of the methods, Mean(M1,M2,M3) are also shown for comparison.

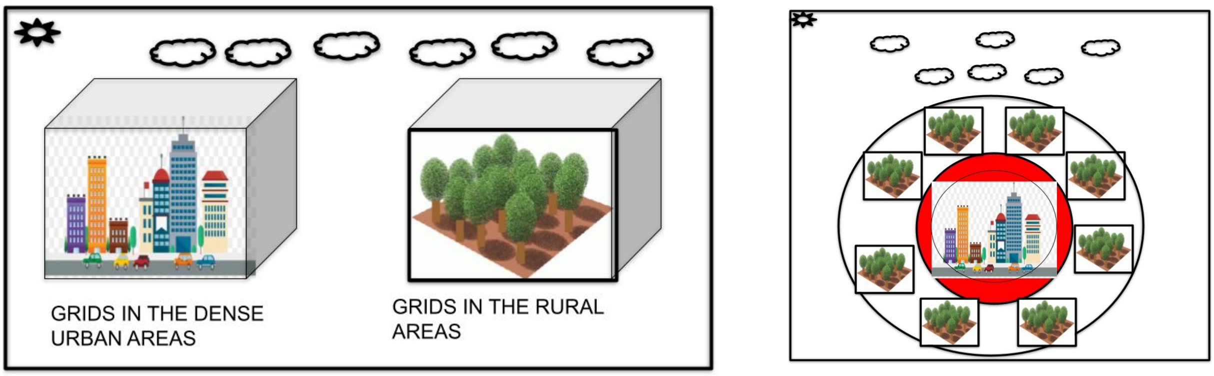

(a) (b)

Figure S1: The figure depicts two common approaches to representing urban and rural areas in urban climate studies: (a) separate grids for urban and rural regions, (b) urban area at the center surrounded by rural grid cells.

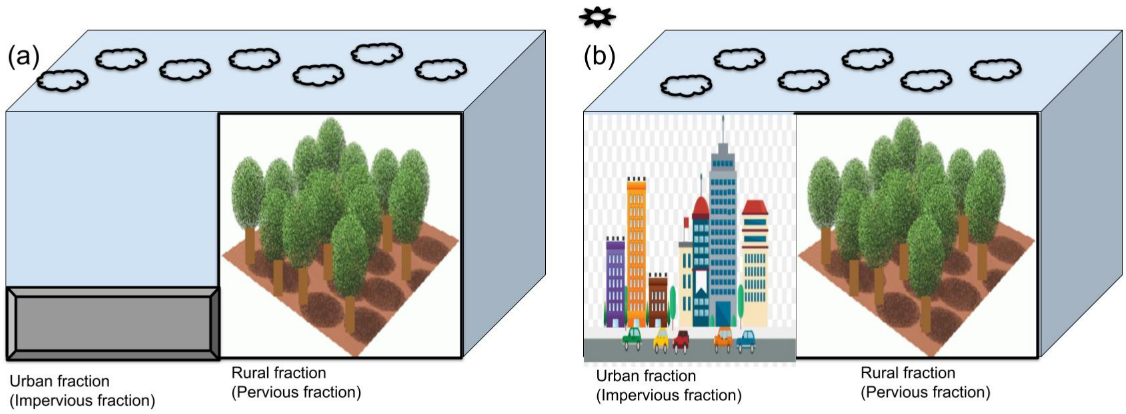

Figure S2: The figure compares two approaches to incorporating urban features into a combined urban-rural grid: (a) a simplified model with adjustments for impervious surfaces like pavement, and (b) a more detailed representation including buildings, roads, and other impervious elements.

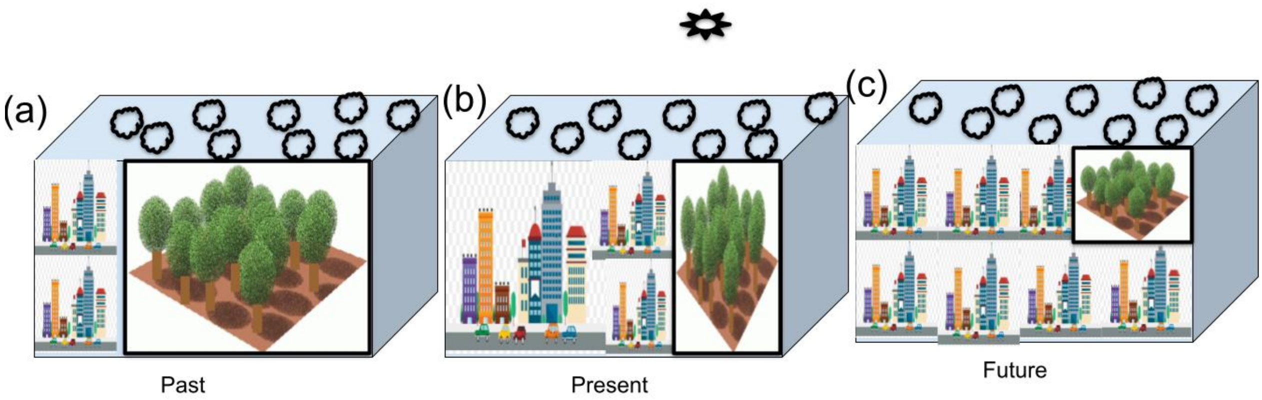

Figure S3: A diagrammatic representation of the hypothetical urban and rural grids in the (a) past (b) present and (c) future. The rural grids decrease from the past to the future as more urban areas are expected to replace most of the natural fractions.

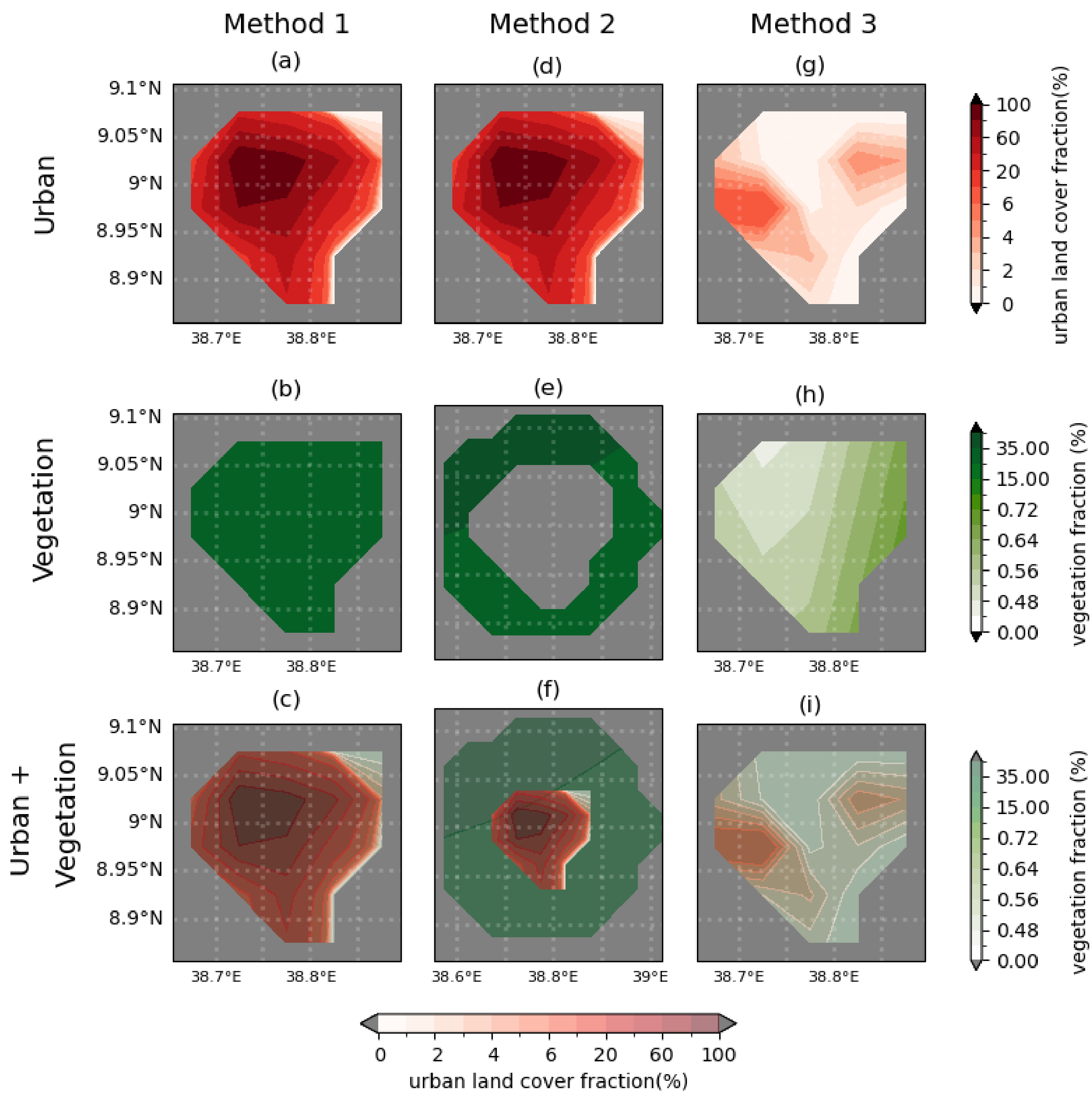

Figure S4: Three frequently used methods to quantify urban and rural properties, Method 1: Urban land cover fractions (a) and vegetation fractions (b) are used to differentiate urban and rural areas, whereas the combined urban and vegetation fractions are shown in (c), Method 2: urban at center (d) and rural areas surrounding it (e) are used to quantify urban and rural properties, whereas the combined Urban and vegetation fractions are shown in (f), and Method 3: Urban dynamics: the differences between urban land cover (g) and vegetation fraction (h) in the first few years (2000-2010) when urban development was low and the next few years (2011-2020) after the city had gone through huge urban development, whereas the combined urban and vegetation dynamics is shown in (i).

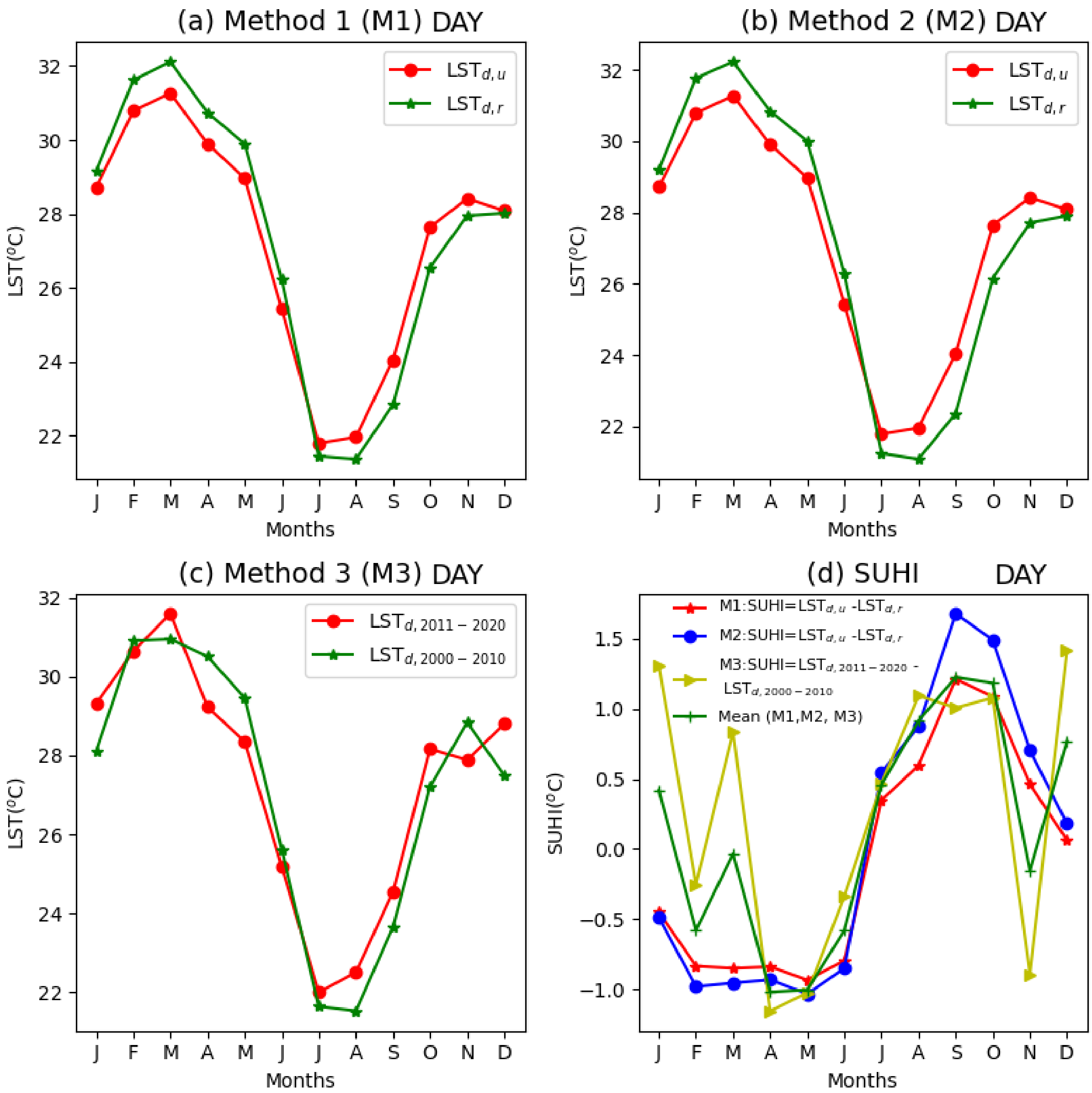

Figure S5: The different methods, (a) method 1, (b) method 2 and (c) method 3, to compute the urban and rural land surface temperature annual cycles. The tropical surface urban heat islands shown in (d) are calculated based on these methods and compared with TSUHI computed from the ground based observation.

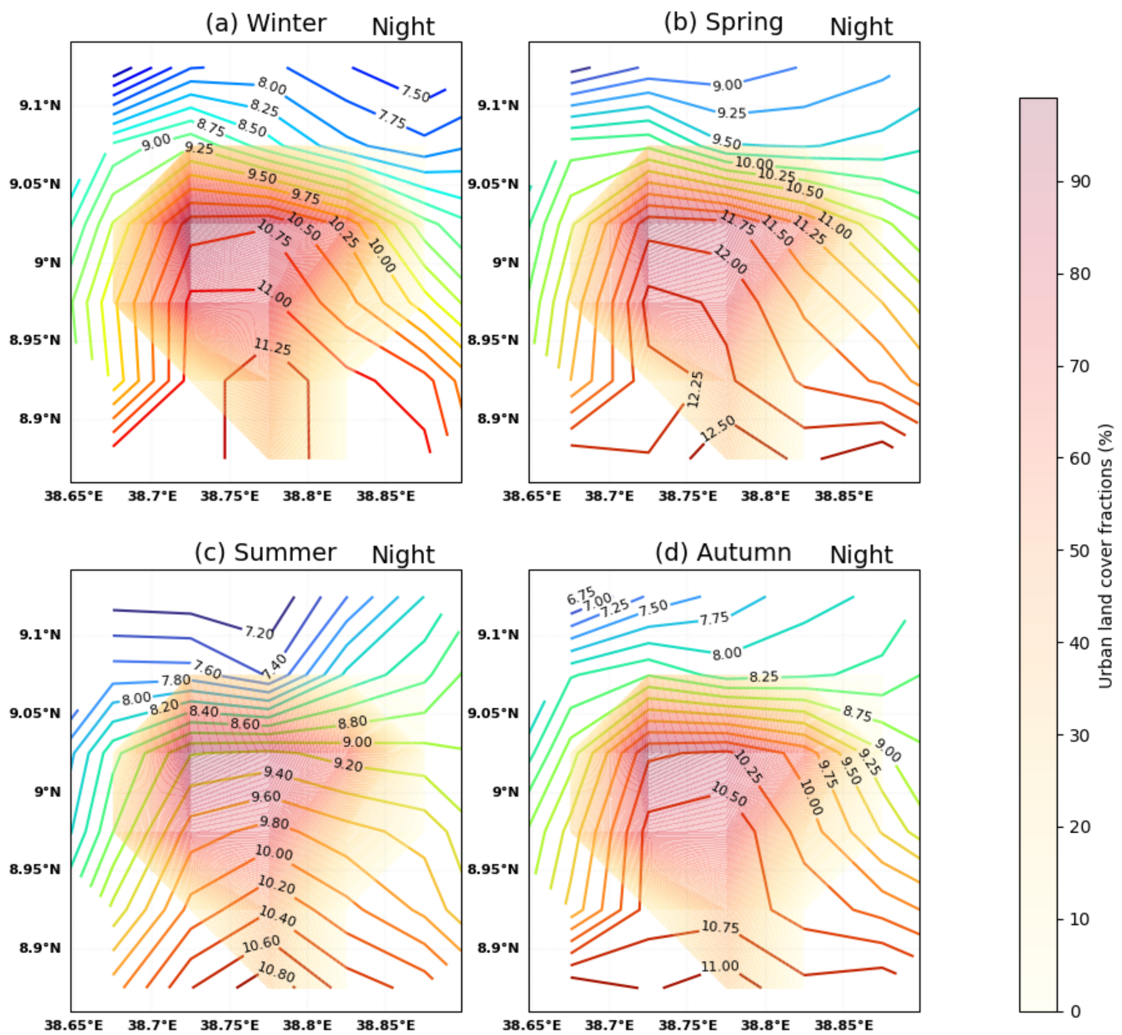

Figure S6: Seasonal mean (2000-2020) MODIS represented land surface temperature contour lines for (a) winter, (b) spring, (c) summer, and (d) autumn seasons during the night time.

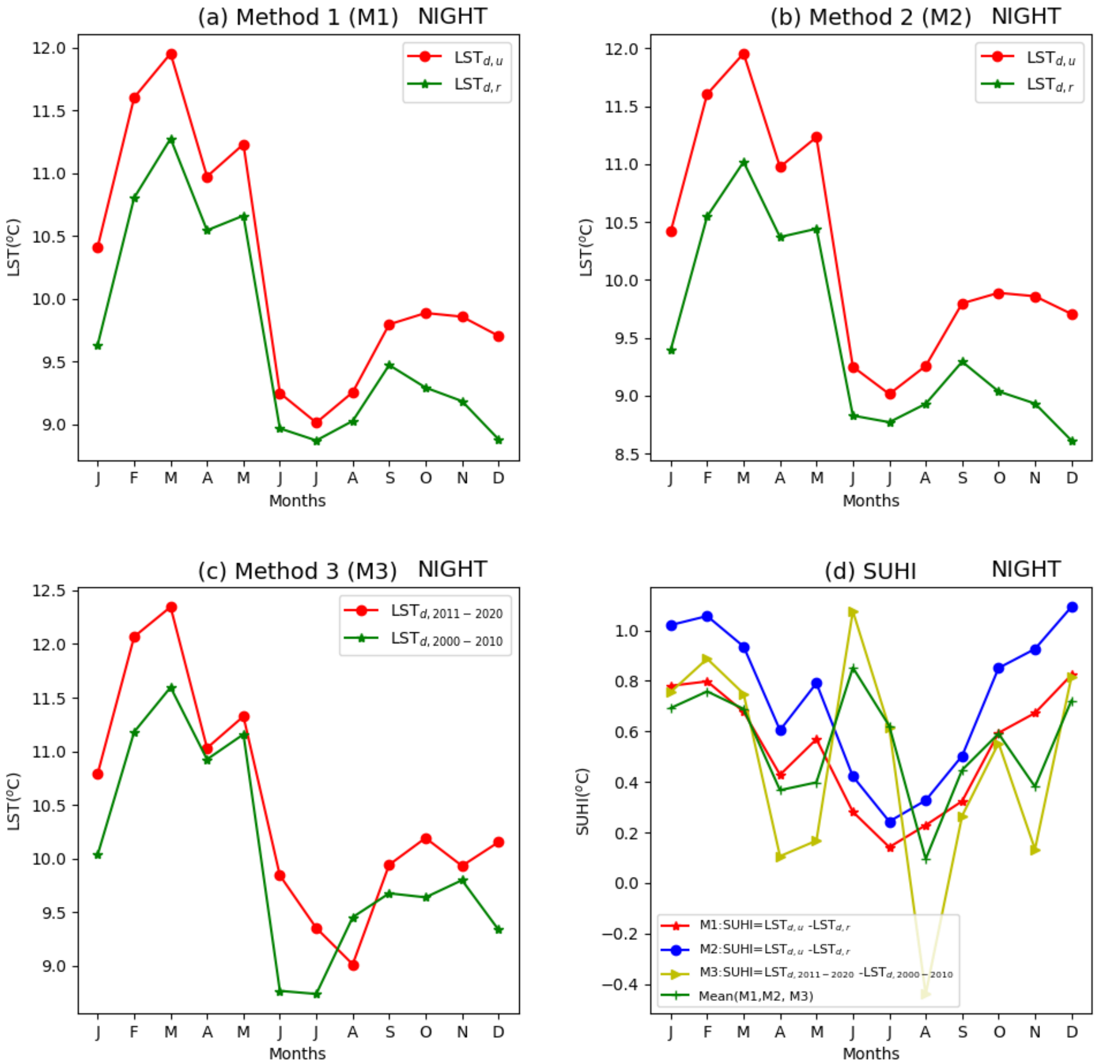

Figure S7: The different methods, (a) method 1, (b) method 2 and (c) method 3, to compute the urban and rural land surface temperature annual cycles during the night. The corresponding nighttime tropical surface urban heat islands are shown in (d).